International Journal of the Physical Sciences Vol. 6(6), pp. 1332-1341, 18 March, 2011
Available online at http://www.academicjournals.org/IJPS
DOI: 10.5897/IJPS10.598
ISSN 1992 - 1950 ©2011 Academic Journals

Full Length Research Paper

An efficient inverter circuit design for driving the ultrasonic welding transducer

Wen-Chung Chang, Sheng-Chien Su and Kai-Hsing Ma*

Department of Electronic Engineering, Southern Taiwan University, Tainan, Taiwan 710, Roc.

Accepted 21 February, 2011

This paper describes a robust circuit design using matching technology to drive the ultrasonic welding transducer with zero voltage switching. A new feedback control method to track the optimal working frequency was practically implemented by a FPGA chip. All analytic results exhibited that the newly designed class-E inverter circuit can be effectively and stably applied on the high power ultrasound welding system.

Key words: Class-E inverter, matching technology, ultrasound welding, zero voltage switching.

INTRODUCTION

Traditional inverter architectures for industrial high power ultrasound systems are including of half-bridge, full-bridge and push-pull circuits (Ishikawa et al., 1997, 1998; Mizutani et al., 1998), which based on conventional complex inverters (class AB or B) (Mortimer et al., 2001). Therefore, to develop a simple and efficient inverter structure is very important for the high power ultrasound systems. In practical application, ultrasound transducer needs a very high resonance quality factor, so the available bandwidth will become very narrow. For most high power ultrasound systems, the characteristics of the mechanical components in the transducer will vary under working condition. Thus, the resonant frequency will be changed for driving high-Q transducers at frequencies other than the transducer resonant frequency results in very small power conversion efficiencies. But for the ultrasound welding system, the working frequency must be in the characteristic capacitive region of piezoelectric transducer. If the working point is too close to the resonance point, the working current will become too large and burn the circuits. This working point application is the difference between the transducer of ultrasound welding system and the other piezoelectric devices. In the high power ultrasound welding system, when the working point is too close to the resonance point, the current changes into very large and makes the system uncontrollable. For industry efficiency application, most of them just simply require the inverter of electrical power into ultrasonic power region. A simple class-E inverter circuit design with zero voltage switching (Raab, 1978; Sokal et al., 1975), which is optimized in the efficiency. The inverter possesses the advantages of simple architecture; low switch voltage and zero voltage switch which make it suitable for the application of power supply system under 500 W. In this research, a simple class-E inverter circuit design is used to drive the ultrasonic welding system.

*Corresponding author. E-mail: khma_710@yahoo.com.tw.

EXPERIMENTAL

Laboratory virtual instrument engineering workbench (LabVIEW) (Jimenez et al., 2005; Lin et al., 2010) supplies a graphical programming environment and can develop the sophisticated measurement, test and control systems by using intuitive graphical icons and wiring the icons to be a control flowchart. As shown in Figure 1, a high power piezoelectric element measurement system includes the LabVIEW program with a computer, a GBIP Interface card, an arbitrary waveform generator (Agilent 33250A), a oscilloscope (Tektronix TDS3000) and a power amplifier (NF HS4012). Generally, the LabVIEW program is regarded as a control interface to measure the piezoelectric characteristic. The GBIP Interface card is used to translate the signals between the waveform generator and the oscilloscope. By the man-machine interface command of the LabVIEW program, the waveform generator will produce and send a frequency signal to the power amplifier (NF HS4012) and enlarge the frequency signal to drive the

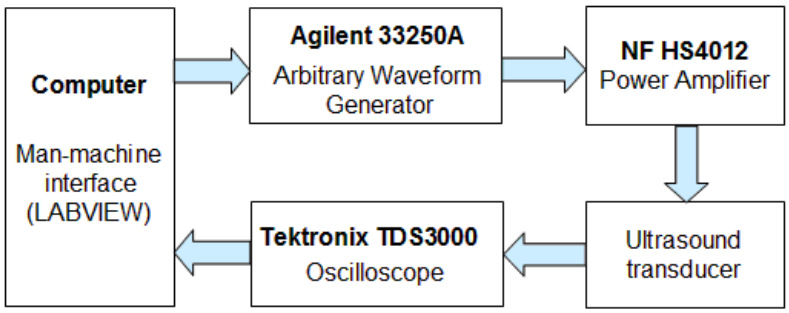

Figure 1. The high power piezoelectric element measurement system.

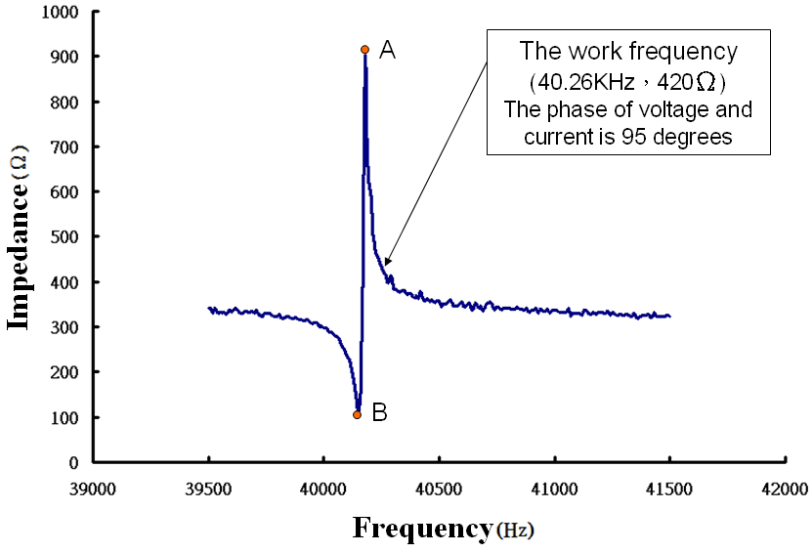

Figure 2. The relation of characteristic impedance vs. frequency.

piezoelectric transducer. By using the GBIP card in the LabVIEW program, it is able to control the oscilloscope to measure the voltage signal and the current signal of the piezoelectric transducer and further to get the impedance of the piezoelectric transducer. During the LabVIEW measurement, the sweeping frequency range is set from 38 to 42 KHz, the sweeping frequency interval is 2 s, the input power for the power amplifier (NF HS4012) is equal to 63.63*1.1 = 70W (at V_{rms}=63.63V, I_{rms}=1.1A), respectively. Then, the piezoelectric feature of transducer can be obtained by frequency sweeping in the high power ultrasound welding system. Typically, these features include the characteristic impedance of the frequency and phase-frequency characteristics, as shown in Figures 2 and 3. In Figure 2, the point B is the resonance point and the point A is the inverse resonance point, respectively.

In this paper, the use of the ultrasound transducer applied to the plastics welding is a piezoelectric material (Rubio et al., 2010) which is produced by the Japan's TDK and applied at very high the power range. Hence, the working point of welding must be stable and controlled in the capacitive region. In other words, the working point voltage and current phase is nearly 90 degrees. As shown in Figure 4, it is found that the impedance characteristic of the piezoelectric transducer will decrease and drift to left while the piezoelectric transducer works at a high temperature (80℃). In other words, the working frequency will be changed and the impedance of the transducer becomes small, while increasing the temperature. The small impedance of the transducer will make the output current become very large immediately. Then, the large output current will raise the output power to burn the mold. Therefore, the ultrasound welding system has to continuously adjust the working frequency to achieve a stable output power.

A class-E inverter circuit design

In Figure 5, the equivalent circuit of a class-E resonant inverter consists a choke inductor L_C, a power switches S, a shunt capacitor C_p and a C_1-L_1-R_L series-resonant circuit (Kazimierczuke et al., 1995). The basic circuit configuration consists a power MOSFET working as a switch, a L_a-C_1-R_L series-resonant circuit, a shunt capacitor C_p, and a chock inductor L_C. The switch turns on and off at the working frequency $f=\omega/(2\pi)$ determined by a driver. The transistor output capacitance, the choke parasitic capacitance, and stray capacitances are included in the shunt capacitance C_p. For high working frequencies, all of capacitance C_p can be supplied by the overall shunt parasitic capacitance. The resistor R_L is an ac

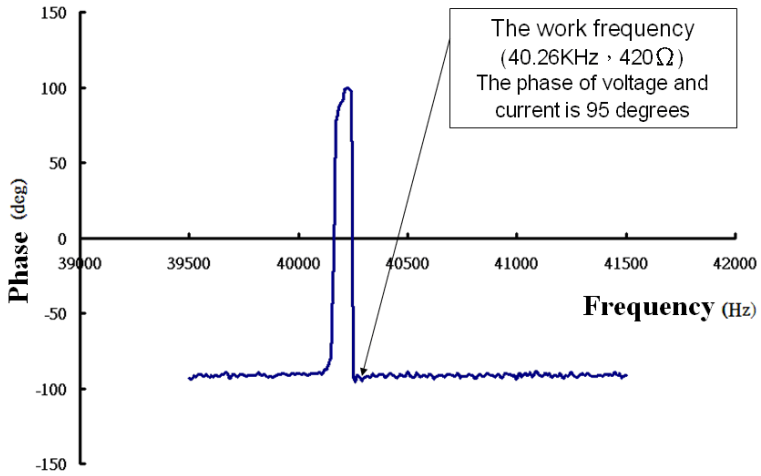

Figure 3. The relation of characteristic phase vs. frequency.

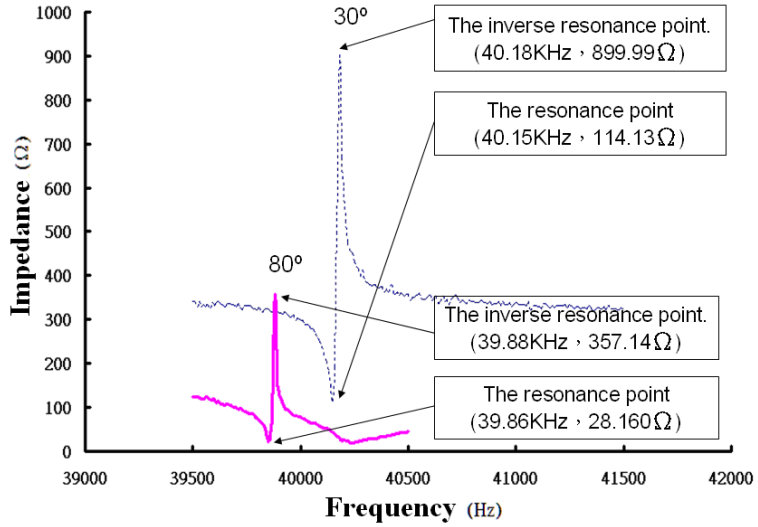

Figure 4. The piezoelectric transducer working at a high temperature (80℃).

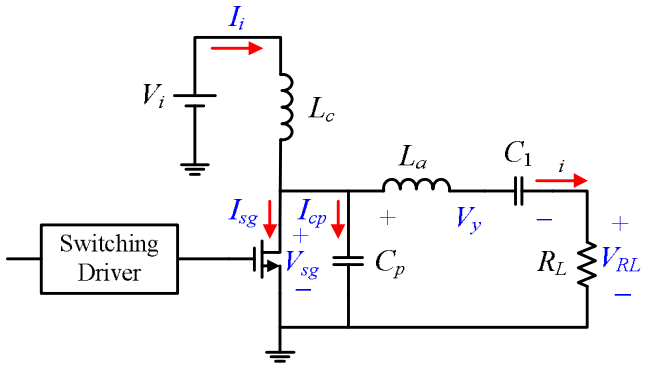

Figure 5. The basic circuit configuration of a class-E resonant inverter.

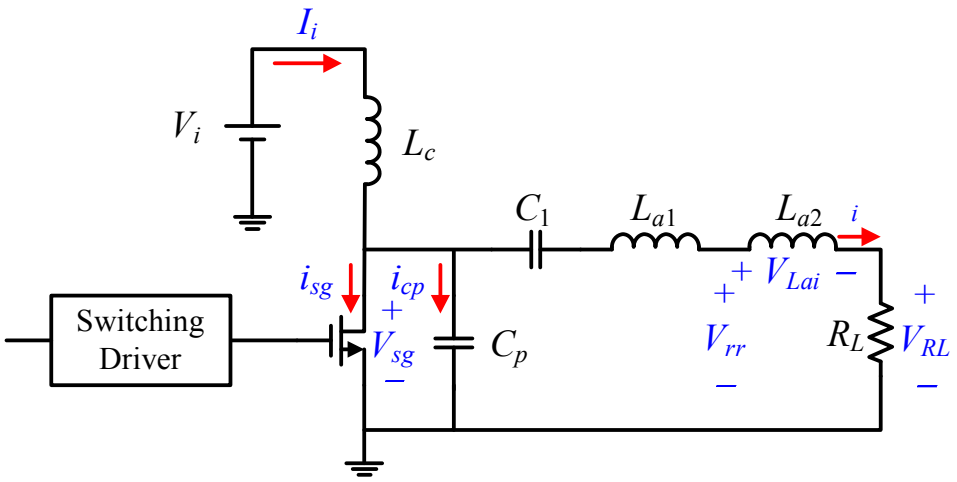

Figure 6. The equivalent circuit of a class-E resonant inverter.

load. The choke inductance L_C is assumed to be high enough so that the ac ripple on the dc supply current Ii can be neglected. A small inductance with a large current ripple is also possible, but the consideration of this case is beyond the scope of this text. When the switch is on, the resonant circuit consists L_a, C_1 and R_L, because the capacitance C_P is short-circuited by the switch. However, when the switch is off, the resonant circuit consists C_P, L_a, C_1, and R_L connected in series. Because C_P and C_1 are connected in series, the equivalent capacitance $C_{eq} = C_1C_P/(C_1 + C_P)$ is lower than C_1 and C_P. The load network is characterized by two resonant frequencies and two loaded quality factors. The switch is on

$$f_{o2} = 1/\left[2\pi\sqrt{L_C C_1 C_P/(C_1 + C_P)}\right] \quad \text{and}$$

$$Q_{L2} = \omega_{o2}L_a/R_L = 1/\left[\omega_{o2}LC_1C_P/(C_1 + C_P)\right] \quad \text{where the}$$

$$f_{o1}/f_{o2} = Q_{L1}/Q_{L2} = \sqrt{C_p/(C_p + C_1)}.$$

Figure 6 shows an equivalent circuit of the inverter for working above resonance. If the working frequency is greater than the resonant frequency f_{o1}, the L_C-C_1-R_L series-resonant circuit represents an inductive load at the working frequency. Therefore, the inductance L can be divided into two inductances, L_{a1} and L_{a2}, connected in series such that $L_a = L_{a1} + L_{a2}$ and L_{a1} resonates with C_1 at the working frequency, that is,

$$\omega = \frac{1}{\sqrt{L_a C}} \tag{1}$$

The loaded quality factor defined at the working frequency is

$$Q_L = \frac{\omega L_a}{R_L} = \frac{\omega(L_{a1} + L_{a2})}{R_L} = \frac{1}{\omega C_1 R_L} + \frac{\omega L_{a2}}{R_L} \tag{2}$$

The current through the series-resonant circuit is sinusoidal and given by

$$i = I_m \sin(\omega t + \phi). \tag{3}$$

where I_m is the amplitude and φ is the initial phase of current. According to Figure 5,

$$i_{Sg} + i_{Cp} = Ii - i = Ii - I_m \sin(\omega t + \phi) \tag{4}$$

For the time interval $0 < \omega t \le 2\pi D$, the switch is on and $i_{Cp} = 0$. Consequently, the current through the MOSFET is given by

$$i_{sg} = \begin{cases} I_{Cp} - I_m \sin(\omega t), & \text{for } 0 < \omega t \le 2\pi D, \\ 0 & \text{for } 2\pi D < \omega t < 2\pi \end{cases} \tag{5}$$

For the time interval $2\pi D < \omega t \le 2\pi$, the switch is off, which implies $i_{Sg} = 0$. Hence, the current through the shunt capacitor C_p is given by

$$i_{Cp} = \begin{cases} 0, & \text{for } 0 < \omega t \le 2\pi D \\ I_i - I_m \sin(\omega t), & \text{for } 2\pi D < \omega t \le 2\pi \end{cases} \tag{6}$$

The voltage across the shunt capacitor and the switch is found as

$$v_{Sg} = \frac{1}{\omega C_p}\int_{2\pi D}^{\omega t} i_{C_1} d(\omega t)$$

$$= \begin{cases} 0, & \text{for } 0 < \omega t \le 2\pi D \\ \frac{1}{\omega C_p}\{I_i(\omega t - 2\pi D) \\ + I_m[\cos(\omega t + \phi) - \cos(2\pi D + \phi)]\}, & \text{for } 2\pi D < \omega t \le 2\pi \end{cases} \tag{7}$$

Substitution of the condition $v_{Sg}(2\pi) = 0$ into (7) yields the relationship among $I_1, I_m, D,$ and φ

$$I_m = I_i \frac{2\pi(1-D)}{\cos(2\pi D+\phi)-\cos\phi} \quad (8)$$

Substitution of (8) into (5) yields the switch current

$$\frac{i_{Sg}}{I_i} = \begin{cases} 1-\dfrac{2\pi(1-D)\sin(\omega t+\varphi)}{\cos(2\pi D+\varphi)-\cos\varphi}, & \text{for } 0<\omega t\le 2\pi D \\ 0, & \text{for } 2\pi D<\omega t\le 2\pi \end{cases} \quad (9)$$

Likewise, substituting (8) into (6). One obtains the current through the shunt capacitor

$$\frac{i_{C_p}}{I_i} = \begin{cases} 0, & for \quad 0<\omega t\le 2\pi D \\ \left[1-\dfrac{2\pi(1-D)\sin(\omega t+\varphi)}{\cos(2\pi D+\varphi)-\cos\varphi}\right] & for \quad 2\pi D<\omega t\le 2\pi \end{cases} \quad (10)$$

From (7), (8) get

$$v_{Sg} = \begin{cases} 0, & \text{for } 0<\omega t\le 2\pi D \\ \dfrac{I_i}{\omega C_p}\left\{\omega t-2\pi D+\dfrac{2\pi(1-D)\left[\cos(\omega t+\varphi)-\cos(2\pi D+\varphi)\right]}{\cos(2\pi D+\varphi)-\cos\varphi}\right\}, & \text{for } 2\pi D<\omega t\le 2\pi \end{cases} \quad (11)$$

Using the condition $dv_{sg}/d(\omega t)=0$ at $\omega t=2\pi$, one obtains the relationship between phase φ and duty cycle D

$$\tan\phi = \frac{\cos 2\pi D-1}{2\pi(1-D)+\sin 2\pi D} \quad (12)$$

From which;

$$\phi = \pi+\arctan\left\{\frac{\cos 2\pi D-1}{2\pi(1-D)+\sin 2\pi D}\right\} \quad (13)$$

From (11), the dc input voltage is found as

$$V_i = \frac{1}{2\pi}\int_{2\pi D}^{2\pi} v_{sg}\,d(\omega t) = \frac{I_i}{\omega C_p}\left\{\frac{(1-D)\left[\pi(1-D)\cos\pi D+\sin\pi D\right]}{\tan(\pi D+\phi)\sin\pi D}\right\} \quad (14)$$

Rearrangement of this produces the input resistance of the class E inverter

$$R_{dc} \equiv \frac{V_I}{I_I} = \frac{(1-D)[\pi(1-D)\cos\pi D+\sin\pi D]}{\omega C_1\tan(\pi D+\phi)\sin\pi D} \quad (15)$$

From (11) and (15), one arrives at the normalized switch voltage waveform

$$\frac{v_{sg}}{V_i} = \begin{cases} 0, \quad \text{for } 0<\omega t\le 2\pi D, \\ \dfrac{\tan(\pi D+\varphi)\sin\pi D}{(1-D)[\pi(1-D)\cos\pi D+\sin\pi D]}\{\omega t-2\pi D+ \\ \quad \dfrac{2\pi(1-D)}{\cos(2\pi D+\varphi)-\cos\varphi}[\cos(\omega t+\varphi)-\cos(2\pi D+\varphi)]\}, \quad \text{for } 2\pi D<\omega t\le 2\pi \end{cases} \quad (16)$$

The current through the series-resonant circuit is sinusoidal. Consequently, higher harmonics of the input power are zero. Therefore, it is sufficient to consider the input impedance of the series-resonant circuit at the working frequency.

Figure 6 shows an equivalent circuit of the series-resonant circuit above resonance at the working frequency. The fundamental component of the input voltage of the series-resonant circuit at the working frequency is

$$v_{rr} = v_{RL} + v_{Lai} = V_{R_{Lm}} \sin(\omega t + \phi) + V_{Laim} \cos(\omega t + \phi) \quad (17)$$

Using (11) and the Fourier formula,

$$V_{RLm} = \frac{1}{\pi} \int_{2\pi D}^{2\pi} v_{sg} \sin(\omega t + \phi) d(\omega t) = -\frac{2 \sin \pi D \sin(\pi D + \phi)}{\pi (1 - D)} V_i \quad (18)$$

Substituting (11) into the Fourier formula and using (14), the amplitude of the fundamental component of voltage the input reactance of the series-resonant circuit (equal to the reactance of the inductance L_{a2}) is obtained as:

$$V_{Laim} = \omega L_{a2} I_m = \frac{1}{\pi} \int_{2\pi D}^{2\pi} v_s \cos(\omega t + \varphi) d(\omega t) \quad (19)$$

$$= \frac{1 - 2(1 - D)^2 \pi^2 + 2 \cos\varphi \cos(2\pi D + \varphi) + \cos 2(\pi D + \varphi)\left[\cos 2\pi D - \pi (1 - D) \sin 2\pi D\right]}{2(1 - D)\pi \cos(\pi D + \varphi)\left[(1 - D)\pi \cos \pi D + \sin \pi D\right]} V_i$$

Combining (8), (16), and (18),

$$\omega C_P R_L = \frac{2 \sin \pi D \cos(\pi D + \varphi) \sin(\pi D + \varphi)\left[(1 - D)\pi \cos \pi D + \sin \pi D\right]}{\pi^2 (1 - D)} \quad (20)$$

Similarly, using (8), (14), and (18),

$$\frac{\omega^2 L_{a2}}{R_L} = \frac{2(1-D)^2 \pi^2 - 1 + 2\cos\varphi\cos(2\pi D + \varphi) - \cos 2(2\pi D + \varphi)\left[\cos 2\pi D - \pi(1-D)\sin 2\pi D\right]}{4 \sin \pi D \cos(\pi D + \varphi)\sin(\pi D + \varphi)\left[(1-D)\pi \cos \pi D + \sin \pi D\right]} \quad (21)$$

The product of (19) and (21) yields

$$\omega^2 L_{a2} C_P = \frac{2(1-D)^2 \pi^2 - 1 + 2\cos\varphi\cos(2\pi D + \varphi) - \cos 2(2\pi D + \varphi)\left[\cos 2\pi D - \pi(1-D)\sin 2\pi D\right]}{2\pi^2 (1-D)} \quad (22)$$

Assuming that the main circuit works in optimal condition that is duty cycle $D = 0.5$, then, the formula can be given as:

$$R_L = 8 / (\pi + 4) \times V i^2 / P_L \quad (23)$$

$$L_a = Q_L R_L / \omega \quad (24)$$

$$C_P = 8 / (\pi(\pi^2 + 4)\omega R_L) \quad (25)$$

$$C_1 = 1 / \omega R_L (Q_L - (\pi(\pi^2 - 4) / 16)) \quad (26)$$

$$L_C = 2(\pi^2 / 4 + 1)(R_L / f) \quad (27)$$

Matching of load

According to the former derivation, R_L among them is replaced as ultrasonic transducer load and need to add matching circuit which can be represented as a matching circuit of transformer-coupled and matching inductance L_b between the class-E and ultrasonic transducer. Normally, the load characteristics are referred to the mechanical side and combined with these elements. The designed class-E inverter is the switching mode and has higher efficiency that can possess low loss and high circuit efficiency than others (for example: class A, AB, B etc.) because of its zero voltage switching characteristic. Ultrasonic transducer is a strong nonlinear time-varying system. Under different working frequency, the difference between impedance characteristics and the mechanical vibration characteristics are remarkable. Most of the ultrasonic welding system works at the region of inductor characteristic to employ the difference with the others applications. The matching

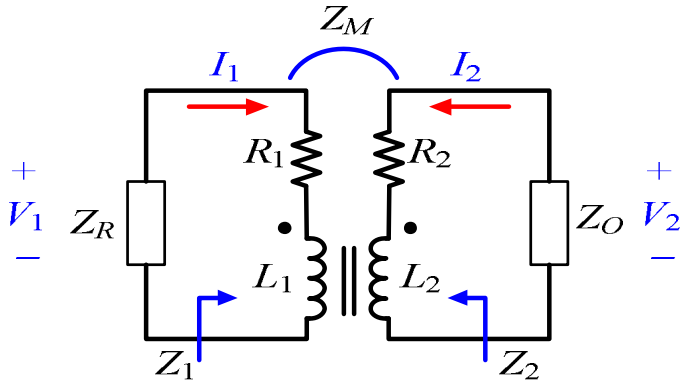

Figure 7. The equivalent circuit of a matching transformer.

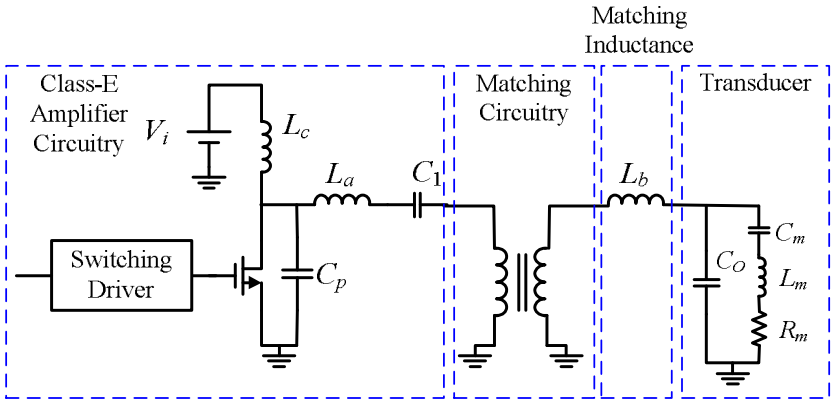

Figure 8. The matching technology of ultrasonic welding system.

transformer design is shown in Figure 7 according to the equivalent impedance with inverter output and ultrasonic transducer input.

The equivalent circuit of a matching transformer is shown in Figure 7. The transformer consists of the primary impendence ($Z_1 = R_1 + j\omega L_1$) of the matching transformer and the secondary impendence ($Z_2 = R_2 + j\omega L_2$) of the matching transformer. L_1 and L_2 are the primary winding and the secondary winding respectively. R_1 and R_2 are parasitic resistances from the loss of the matching transformer material and winding. Z_R and Z_o are the input primary impedance and the output secondary impedance respectively. Z_M is the mutual coupling impendence of the matching transformer which consists of R_M and $j\omega L_M$ where R_M is the mutual coupling resistance; L_M is the mutual coupling inductor. V_1 and I_1 are the input voltage and current respectively. V_2 and I_2 are the output voltage and current respectively. The voltage and current relation equations of the matching transformer circuits in Figure 8 are

$$V_1 = I_1 Z_1 - Z_M I_2 = I_1 Z_R$$
$$V_2 = I_2 Z_2 - Z_M I_1 = I_1 Z_O \quad (28)$$

By using (28), we can obtain Z_R.

$$Z_R = Z_1 - \left(Z_M^2 / (Z_2 + Z_0)\right) \quad (29)$$

When circuit of the secondary impendence is short ($Z_O = 0$), we can get the input primary impendence Z_{RO}. By using equation (29), the Z_M is

$$Z_M = \left[Z_2 (Z_1 - Z_{R0})\right]^{1/2} \quad (30)$$

By using equation (29) and (30), we can get Z_R, Z_O and the output secondary admittance Y_O.

$Z_R = (Z_O Z_2 + Z_1 Z_{RO}) / (Z_O + Z_1)$ and $Z_O = [Z_2 (Z_R - Z_{RO})] / (Z_1 - Z_R)$

$$Y_0 = \frac{1}{Z_0} = G_0 + jB_0 = \frac{\frac{Z_1}{Z_2} - \frac{Z_R}{Z_2}}{R - Z_{RO}} \quad (31)$$

We assumed the primary impendence is a pure resistance ($Z_R = R$), the output secondary admittance ($G_o + jB_o$) is

$$G_0 + jB_0 = \frac{\frac{Z_1}{Z_2} - \frac{R}{Z_2}}{R - Z_{RO}} \quad (32)$$

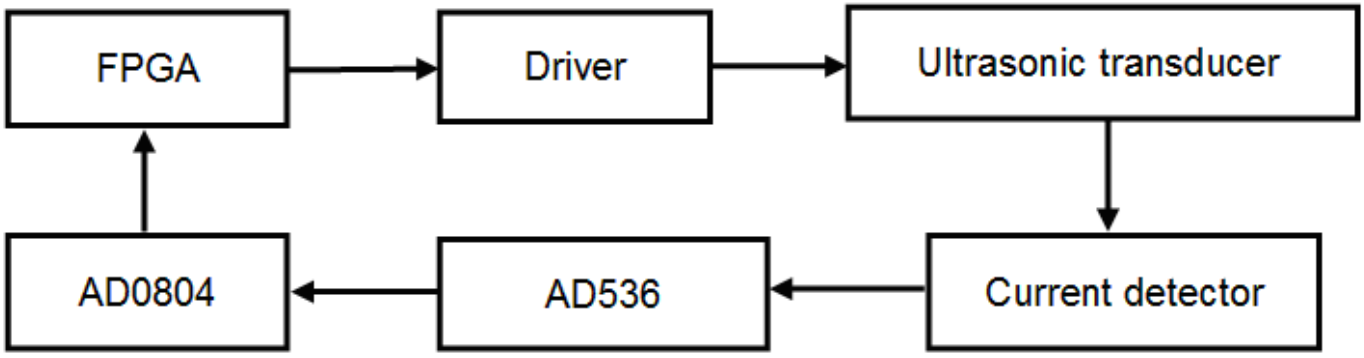

Figure 9. The overall blocks of the driving system.

We assumed R_1, R_2 are extremely small (near to zero), the transformer impendence ratio ($n = Z_1/Z_2$) is

$$n = \frac{R_1 + j\omega_O L_1}{R_2 + j\omega_O L_2} \cong \frac{j\omega_O L_1}{j\omega_O L_2} \cong \frac{L_1}{L_2} \quad (33)$$

We assumed $|Z_{RO}| << R$, the output secondary admittance is

$$G_0 + jB_0 = n\frac{1}{R} + \frac{1}{j\omega L_2}$$

$$n = RG_0 \Rightarrow L_2 = \frac{1}{W_0 B_0} \Rightarrow L_1 = \frac{RG_0}{W_0 B_0} \quad (34)$$

To adjust repeatedly L_a and L_b for the output waveform of the voltage and current and the impedance matching of matching circuit is mainly in order to deliver the suitable power from inverter to ultrasonic transducer. L_b is the matching inductor in the matching network which used ultrasonic coupling technology. Therefore, the selection of appropriate matching circuit parameters has a very important significance.

RESULTS AND DISCUSSION

The frequency tracking circuit measuring frequency range is from 39.5 to 40 KHz. The resonance frequency is 39.75 KHz at the lowest impedance. The setting is to make the system work at the optimal working frequencies with ultimate stability. The feedback control method of ultrasound welding system is implemented with a VHDL program in a FPGA chip. The FPGA chip has two major logic circuits. One logic circuit is designed to sweep and catch the working frequency. The other logic circuit is designed to adjust the working frequency simultaneously. In this study, the feedback controlling method of an ultrasonic machine at the working frequency (40 KHz) and the working power (550 W) are controlled by the output current value. The overall blocks of the driving system are shown in Figure 9.

In the main system, AD0804 communicates with the FPGA chip through an AD536 to detect the amount of working current and is controlled by the data from output current of the ultrasonic welding system. The function of AD536 can be fetched any alternating signal to change into root mean square (RMS) value. Then, the current threshold is set and transmitted to the FPGA chip to launch the frequency-sweeping circuit. When repeating the sweeping of ultrasonic transducer frequency, the chip catches the ultrasonic working frequency simultaneously. The control module will sweep several frequency ranges in sequence with the default sweeping time to access the working frequency value. Then, the normal working frequency value is sent to the driver. At this point, the current value of the working current is smaller or the same as the default threshold.

As shown in Figure 10, the class-E inverter for ultrasonic welding system (40 KHz and 500 W) which possesses the high efficiency with zero voltage switching. The driving circuit parameters of ultrasonic welding system with feedback design used in the experiments are shown in Table 1. If the ultrasonic welding system becomes unstable, the output voltage of power driving circuit will be greatly reduced due to the leading of loading and thermal effects than the shift of working frequency. The detecting circuit will measure the output voltage of the power driving circuit using the technology of class-E combined with transformer matching circuit. It possess the self-adjust function where the interference resulted from the load effect of transducer for ultrasonic welding system. The graph of the output waveform of the ultrasonic welding system is shown in Figure 11. The results present the typical voltage and current waveforms for this type of welding transducer.

In this kind of design, the ultrasound welding system working in the capacity range will be easy to steady control and not rise the temperature which results in the very low power assumption. The efficiency comparisons between the simple class-E inverter circuit and the traditional inverter circuit with 50 test times in the

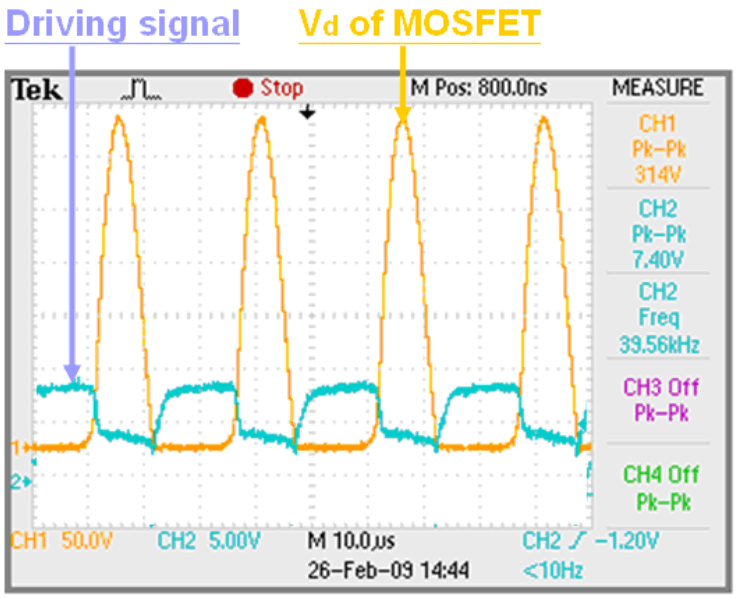

Figure 10. The zero voltage switching condition.

Table 1. The driving circuit parameters in the designed ultrasonic welding system.

Design element	Value of parameter
L_C	1.5 mH
L_a	1.0 mH
L_b	0.5 mH
C_P	18 nF
Tr	9.3 mH:15 mH

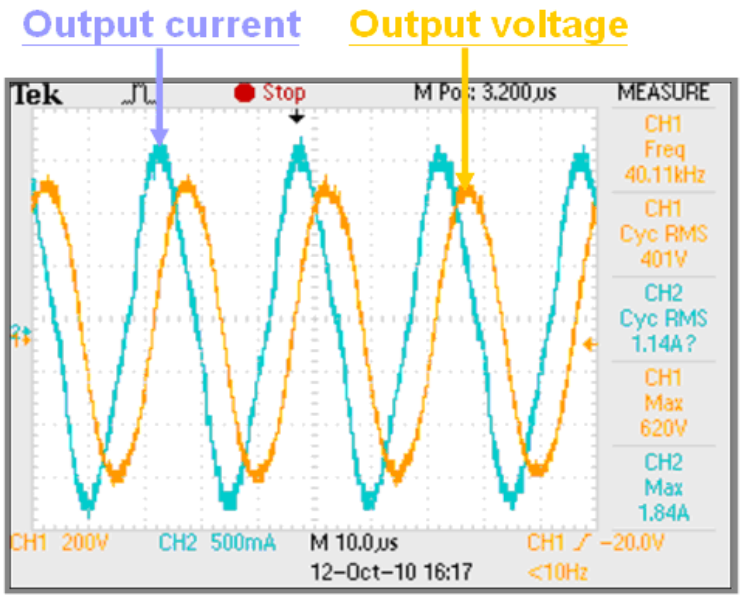

Figure 11. The ultrasonic output of the class-E welding system.

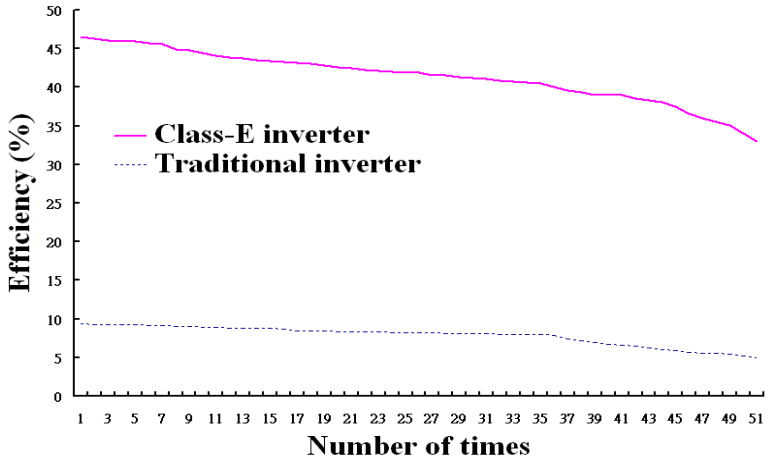

Figure 12. The efficiency comparisons of the ultrasound welding system between the simple class-E inverter circuit and the traditional inverter circuit during 50 test times.

ultrasound welding system are shown in Figure 12. It is found that the efficiency of the class-E inverter circuit design in the ultrasound welding system is more remarkable stable than that of traditional inverter circuit. This is because the class-E inverter circuit design can raise the efficiency to make the output power into a more stable region and get a longer system life time.

Conclusion

A class-E resonant inverter incorporated with a matching transformer method to drive the ultrasonic welding system with zero voltage switching is successfully developed. A simple inverter characteristic model and a feedback control with a CPLD chip are both used to derive the optimal parameters for the system state stability. This control method is implemented on a practical ultrasound welding system currently used inindustry applications. The results prove that this kind of class-E circuit can be succeed with a new feedback control to drive high power effectively and automatically track a proper frequency for the ultrasound welding system.

ACKNOWLEDGEMENT

The authors would like to express thanks to professor Kao-Feng Yarn, Far East University for his beneficial discussion and kindly help in writing this paper.

REFERENCES

Jimenez FJ, De Frutos J (2005). Virtual instrument for measurement, processing data and visualization of vibration patterns of piezoelectric devices. Comp. Standards Interfaces, 27: 653-663.

Ishikawa J, Mizutani Y, Suzuki T, Ikeda H, Yoshida H (1997). High-frequency drive-power and frequency control for ultrasonic transducer operating at 3MHz. IEEE Industry Applications Conference and Thirty-Second IAS Annual Meeting, 2: 900-905.

Ishikawa J, Sato T, Suzuki T, Ikeda H, Yoshida H, Shinohara S (1998). New type of compact control system for frequency and power in megasonic transducer drive at 1MHz. IEEE Industry Applications Conference and Thirty-Second IAS Annual Meeting, 3: 1638-1643.

Lin WB, Yarn KF, Shih KR (2010). LabVIEW implement for distorted signal detection with robust complex extended Kalman filter. Int. J. Phy. Sci., 5: 2161–2170.

Mizutani Y, Suzuki T, Ikeda H, Yoshida H, Shinohara S (1998). Frequency control of MOS-FET full bridge power inverter for maximizing output power to megasonic transducer at 3MHz. IEEE Industry Applications Conference and Thirty-Second IAS Annual Meeting, 3: 1644-1651.

Mortimer B, Bruyn T, Davies J, Tapson J (2001). High power resonant tracking amplifier using admittance locking. Ultrasonics, 39: 257-261.

Raab FH (1978). Effects of circuit variations on the class-E tuned power amplifier. IEEE J. Solid-State Circuits. 13: 239-247.

Rubio TO, Buiochi F, Adamowski JC (2010). Topology optimized design of functionally graded piezoelectric ultrasonic transducers. Phys. Procedia. 3: 891-896.

Sokal NO, Sokal AD (1975). Class E-A new class of efficiency tuned single-ended switching power amplifiers. IEEE J. Solid-State Circuits. 3: 168-176.

Kazimierczuke MK, Czarkowski D (1995). Resonant Power Converter, (New York Wiley).